Surfaces and Interfaces 76 (2025) 107943

Contents lists available at ScienceDirect

Surfaces and Interfaces

journal homepage: www.sciencedirect.com/journal/surfaces-and-interfaces

Plasma-tailored SPCEs for enhanced surface reactivity and electron transfer: Toward improved electrodes

Sunil Luhar *, Kamila Sadowska *

Nalecz Institute of Biocybernetics and Biomedical Engineering, Polish Academy of Sciences, Ks. Trojdena 4, 02–109 Warsaw, Poland

ARTICLE INFO

Keywords:
Plasma treatment
Electrode
Wettability surface engineering
Electrochemical impedance spectroscopy
Diffusion processes
Predictive model

ABSTRACT

Carbon-based electrodes have emerged as essential components in modern electrochemical systems because of their outstanding electrical conductivity, chemical stability, and customizable surface characteristics. In this study, we explore the impact of oxygen plasma treatment on the surface properties of screen-printed carbon electrodes (SPCE). Plasma exposure durations of 1, 3, and 5 min were applied to systematically investigate the extent of surface modification. The treatment effectively introduces oxygen-containing functional groups, thereby enhancing surface wettability, promoting faster electron transfer kinetics, and improving overall electrochemical performance. Comprehensive characterization was performed using X-ray photoelectron spectroscopy (XPS), scanning electron microscopy (SEM), cyclic voltammetry (CV), and electrochemical impedance spectroscopy (EIS). Additionally, contact angle measurements were conducted to assess changes in hydrophilicity. To correlate wettability with electrochemical behavior, a predictive model was developed in which both the electrochemically active surface area (ECSA) and electron transfer rate constant (k_{et}) scale with $\cos(\theta)/R_{ct}$. The results demonstrate that oxygen plasma treatment significantly increases the number of surface polar groups and reduces the charge transfer resistance. These findings highlight the potential of plasma-based surface engineering as a powerful and environmentally friendly strategy to optimize the SPCE for high-performance applications in electrochemistry.

1. Introduction

Electrochemical technologies are at the forefront of next-generation sensing, energy storage, and catalysis platforms [1,2]. Central to these technologies carbon-based electrodes [3], such as screen-printed carbon electrodes (SPCEs) [4], plastic chip electrodes (PCEs) [5], boron-doped diamond electrodes (BDDs) [6] and some flexible carbon-modified electrodes, are used in various applications [7]. Among these, SPCEs are widely used in various electrochemical applications because of their outstanding electrical conductivity, chemical stability, versatility, cost-effectiveness and customizable surface properties [8]. However, the electrochemical performance of the electrodes strongly depends on their surface characteristics, including functional groups, roughness, and wettability [9,10]. To enhance their performance, SPCEs require surface modification [11,12]. A variety of techniques have been explored to tune the properties of SPCEs, including chemical functionalization, coating, and electrochemical treatments [13–15]. Among these methods, plasma treatment has gained significant attention as a highly effective and environmentally friendly approach [16–18]. Surface modification is essential for improving the electrochemical behaviour of SPCEs, as it influences key factors such as the diffusion coefficient, electron transfer rate, and overall sensitivity of the electrode [19,20]. These factors are directly related to surface conditions, which can be altered by the introduction of molecular recognition elements and blocking materials [21]. While electrochemical activation methods, such as the application of specific potentials in acidic or buffered solutions, can generate functional groups such as carboxyl groups for covalent bonding, they often have limitations in terms of process complexity and scalability [22,23].

In contrast, plasma treatment-especially oxygen plasma treatment-has emerged as a highly convenient and efficient method. This process involves exposing the SPCE surface to oxygen plasma, which introduces oxygen-containing functional groups [24] (such as hydroxyl, carboxyl, and carbonyl groups) onto the electrode surface [25,26]. These modifications significantly improve the hydrophilicity, polar group, and electron transfer kinetics of the electrode, thereby enhancing its performance in applications such as biosensors, supercapacitors, and electrocatalysis [27,28]. The simplicity, scalability, and environmental

* Corresponding authors.
E-mail addresses: sluhar@ibib.waw.pl (S. Luhar), ksadowska@ibib.waw.pl (K. Sadowska).

https://doi.org/10.1016/j.surfin.2025.107943
Received 29 May 2025; Received in revised form 4 September 2025; Accepted 23 October 2025
Available online 25 October 2025

friendliness of plasma treatment make it an ideal choice for surface modification [29–31], as it not only enhances the electrochemical properties but also facilitates surface cleaning and regeneration, ensuring optimal performance in various electrochemical systems [32, 33].

This study introduces a novel, time-controlled approach to modifying screen-printed carbon electrodes (SPCEs) using oxygen plasma treatment, with exposure durations of 1, 3, and 5 min. Unlike previous studies that often apply surface treatments without systematic optimization, our work explores the temporal effects of plasma exposure on SPCE surface properties in a controlled manner. A comprehensive set of advanced characterization techniques, including SEM-EDX, AFM, XPS, ATR-FTIR, contact angle measurements, cyclic voltammetry (CV), and electrochemical impedance spectroscopy (EIS), was employed to correlate morphological, chemical, and electrochemical changes in detail. Importantly, the stability of the modified electrodes was evaluated over a 20-day period, addressing a critical but often overlooked aspect of practical electrode application. Furthermore, we propose a predictive model that quantitatively links surface characteristics with electrochemical behavior, offering a valuable framework for optimizing SPCE performance in future sensor and analytical device development.

2. Materials and methods

2.1. Materials and apparatus

Commercial SPCEs, specifically graphite screen-printed electrodes (Gr-SPE), were purchased from EcoBioService (Italy). As specified by the producer, each electrode is produced by screen-printing technology and consists of a round-shaped graphite working electrode (3 mm diameter), a silver/silver chloride pseudo-reference electrode and a graphite counter electrode. All chemicals used were of analytical grade and were employed without further purification. The following reagents were obtained from Chempur, Poland: disodium hydrogen phosphate (Na_2HPO_4), potassium dihydrogen phosphate (KH_2PO_4), potassium chloride (KCl), sodium chloride (NaCl), potassium hexacyanoferrate(III) (K_3 [Fe(CN)$_6$], ≥99 %),and potassium hexacyanoferrate(II) trihydrate (K_4 [Fe(CN)$_6$]·3H$_2$O). Deionized water (resistivity: 18.2 MΩ·cm) was obtained via a reverse osmosis system and used throughout all the experiments.

Electrochemical studies were performed using a PalmSens potentiostat/galvanostat system (PalmSens BV, The Netherlands) operated with PSTrace 5.59 software. Two electrochemical techniques were employed: CV, and EIS. Scanning electron microscope ZEISS CrossBeam 540 equipped with energy dispersive X-ray spectroscopy detector (Bruker) was used. Static contact angle measurements were carried out using a DSA25 Drop Shape Analyser (KRÜSS GmbH, Hamburg, Germany) with deionized water droplets of 5 μL volume. The ATR-FTIR measurements were performed using the Thermo Scientific Nicolet Summit X FTIR Spectrometer with the Everest ATR accessory. The surface of SPCEs was studied with XPS using the Kratos Axis Supra spectrometer equipped with a monochromatic Al Kα radiation (1486.7 eV) source. The spot size of a single analysis was 300 μm × 700 μm. The peak fitting was done with the CasaXPS software version 2.3.18 on a Shirley background. All spectra were calibrated using the C 1 s peak with a fixed value of 284.4 eV. AFM measurements were performed using a Combi-Scope™-1000 SPM system (AIST-NT).

2.2. Oxygen plasma treatment

SPCEs were treated with oxygen plasma using a HARRICK PLASMA cleaner. The treatment was carried out at a power setting of 0.30 W, with the radio frequency (RF) power level set to medium. The flow rate of oxygen gas was maintained at 0.5 SCFH, and the operating pressure was set to 575 Torr. The electrodes were subjected to plasma treatment for varying durations of 1, 3, and 5 min and the samples were labelled 1 SPCE, 3 SPCE and 5 SPCE. During the plasma treatment process, the SPCE electrodes were placed on a glass substrate to ensure uniform exposure to the plasma. After treatment, the electrodes were stored in a desiccator to prevent moisture absorption and to preserve their properties until further analysis.

3. Results and discussion

3.1. Physical characterization

3.1.1. SEM/AFM

The surface morphologies of the pristine electrode (SPCE) and the plasma-treated electrodes (1 SPCE, 3 SPCE and 5 SPCE) were analysed using SEM and AFM. As shown in Fig. 1 and Figs. S1 and S2 in the Supplementary file, the SEM image of the pristine SPCE reveals relatively uniform, densely packed carbon particles, characteristic of screen-printing processes. Limited number of pores and cracks can be seen. After plasma treatment, surface became rougher and more granular as compared to SPCE. Increased presence of micro-voids and surface irregularities, with more distinguishable boundaries and cracks can be observed. AFM analysis further supported these observations (see Fig. S3). The pristine SPCE has an average surface roughness (R_a) of 15.7 nm and a root mean square roughness (RMS) of 19.9 nm. After 1 min of plasma treatment, the roughness significantly increased, with R_a reaching 23.8 nm and the RMS increasing to 30.6 nm. For sample 3 SPCE and 5 SPCE R_a equals to 17.3 nm and 23.0 nm, respectively, with RMS of 22.3 and 29.6 nm, respectively. Analysing the results, it can be concluded, that plasma treatment can peel-off carbon layer in some period of time, and 1 min of plasma treatment changes porosity and the roughness at the highest level. This is enough to remove surface impurities and uncover graphite layers, keeping however the uniformity of the electrode area. Higher RMS and R_a values often correlate with better sensor sensitivity in electrochemical applications, due to increased active surface area and electron transfer sites, which was further proved in electrochemical analysis.

3.1.2. Elemental analysis

XPS was utilized to investigate the surface elemental composition and chemical states of the pristine SPCE, 1 SPCE, 3 SPCE and 5 SPCE. All the spectra were normalized and deconvoluted, with a detailed focus on the C 1s and O 1s regions, as shown in Fig. 2. The survey spectrum of the pristine SPCE (Fig. 2A) reveals that the surface primarily comprises carbon and oxygen, with some amounts of chlorine (c.a. 5 %), likely originating from manufacturing residues such as solvents or components of the Ag/AgCl reference electrode ink. Carbon is the most abundant element, which is consistent with a graphitic surface composition [34]. The deconvolution of the C 1s region (Fig. 2a) displays a dominant peak at 285.5 eV attributed to graphitic C=C bonds, along with a significant contribution (~29 %) from sp^3 hybridized carbon (C–C/C–H), suggesting the chemisorption of hydrogen. The O 1s region (Fig. 2a1) indicates the presence of hydroxyl (C–OH) and carboxylic acid (O–C=O) groups at ratios ranging from approximately 61.7 % to 38.3 %, respectively. Contact angle measurements (Fig. 4) support the hydrophobic nature of the untreated SPCE surface. After plasma treatment (1 SPCE, 3 SPCE and 5 SPCE), there was a slight reduction in the total carbon content and a notable increase in the oxygen concentration (see Table 1 and Fig. 2 A) indicating successful surface oxidation and functionalization. The C/O ratio for SPCE was equal to c.a. 17 and was substantially reduced after plasma treatment (C/O ≈ 6) Notably, the amount of chlorine was also reduced for all plasma-treated samples, proving effective cleaning action of plasma. Detailed analysis of C 1s and O 1s spectra of 1 SPCE, 3 SPCE and 5 SPCE samples revealed some changes in their chemical composition. The C 1 s spectra of 1 SPCE, 3 SPCE and 5 SPCE sample, (Fig. 2 b,c and d) show a noticeable decrease in the sp^3 carbon content (C–C/C–H reduced to ~1.2 %, 0.38 % and 3.2 %, respectively), highlighting the effective removal of surface hydrocarbons by plasma etching. The

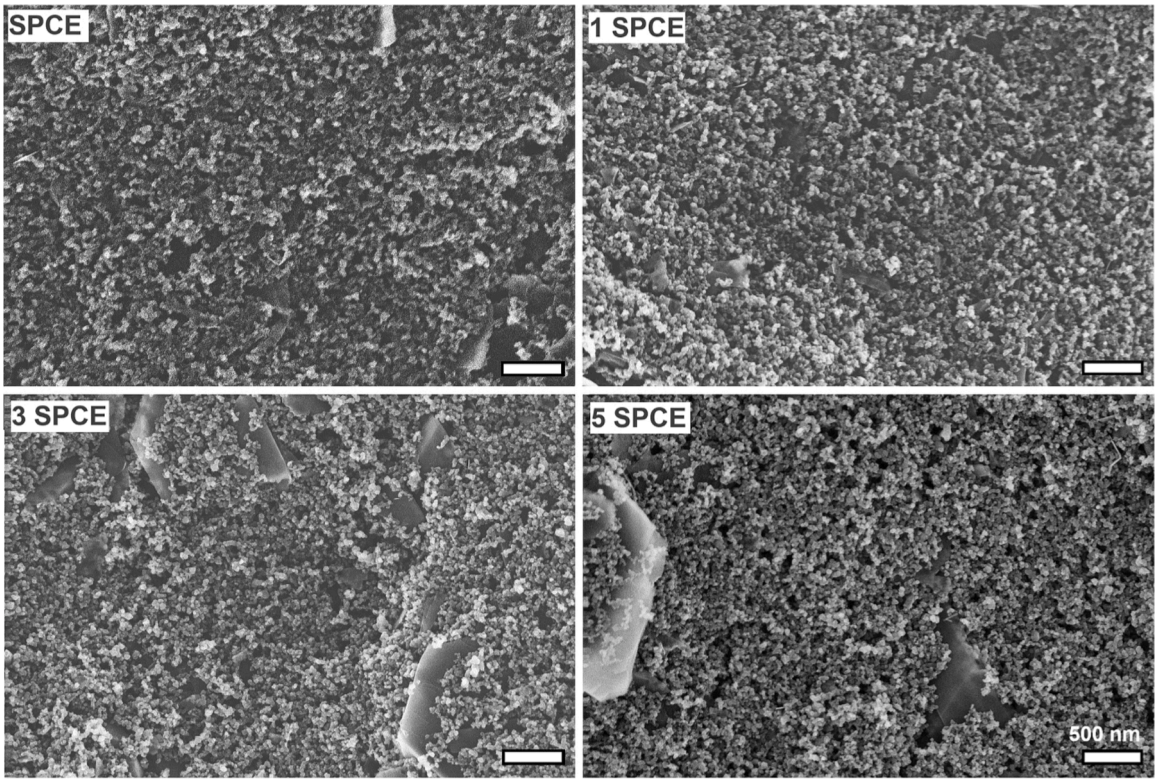

Fig. 1. SEM images of pristine SPCE and plasma treated samples (1 SPCE, 3 SPCE and 5 SPCE).

prominent graphitic C=C peak is retained, accompanied by an increased presence of C–OH and O–C=O groups, confirming the introduction of oxygen-containing functionalities. Oxygen plasma is a highly reactive form of oxygen created by applying energy to O_2 molecules, leading to their ionization and dissociation into a mixture of reactive species. Oxygen plasma consists of neutral species (atomic oxygen, molecular oxygen, and ozone), ions (O_2^+, O^+, and O^-), excited species and free electrons. Plasma species play a critical role in selectively removing sp^3 carbon, contributing to surface purification, structural ordering, and improved electronic properties [32,35]. The selectivity arises due to differences in bond strength, reactivity, and local energy absorption between sp^2 and sp^3 carbons. Plasma-generated species (e.g., $O\cdot$, O_2^+) are more likely to break weaker sp^3 C–H bonds first, resulting in selective etching of these regions. It is well seen in the XPS results: a reduced C–C (sp^3) peak and increased C=C (sp^2) content was observed for plasma-treated samples, confirming chemical selectivity. Moreover, reactive oxygen radicals preferentially oxidize sp^3 carbon to form oxygen-containing functional group (e.g. carbonyl, carboxyl, hydroxyl), which was also evidenced by XPS analysis. As can be seen in Fig. 2A, O 1s signal displays a significant increase in intensity. The detailed analysis of O 1s spectra of 1 SPCE, 3 SPCE and 5 SPCE showed increased contributions from hydroxyl, carboxylic acid, and newly appearing peaks corresponding to adsorbed water (H_2O). This supports a transition from a hydrophobic to a hydrophilic surface. Analysing the data for O 1s region, summarized in Table 2, some trend can be observed. There is a clear shift from hydroxyl-dominant to carboxyl-dominant oxygen chemistry for increased time of plasma treatment. Gradual loss and/or transformation of hydroxyl groups to more stable lactones and quinones occurs. According to the well-known reactions, phenol/catechol groups that are placed on the edges of the graphite sheets can be further converted into quinone groups. Moreover, prolonged exposure to O_2 plasma (5 min) can cause carboxyl groups located near hydroxyl groups to undergo condensation, forming lactone structures. This process involves the elimination of a water molecule, resulting in the loss of one oxygen atom. Consequently, a decrease in the overall oxygen atomic content is expected in 5 SPCE sample, along with increased content of O-C=O, which aligns with the data presented in Table 1 and Table 2 for 5 SPCE. We observed similar behaviour for reduced graphene oxide as reported previously in [36]. Overall, the progressive plasma treatment effectively increased the surface density of the oxygen-containing groups. This modification enhanced surface wettability and reactivity and is expected to improve the electrochemical performance of the SPCE. These results, summarized in Fig. 2 and Tables 1 and 2, clearly demonstrate that oxygen plasma treatment is a successful strategy for surface cleaning, oxidation, and functionalization of SPCE.

Additionally, we performed EDX analysis which typically probes deeper into the sample and thus showed remarkable differences as compared to XPS data. The results are summarized in Table 3. The oxygen content slightly increased after plasma treatment (1 SPCE, 3 SPCE and 5 SPCE) as compared to pristine SPCE. Small differences in the oxygen content among samples indicate, that the functionalization occurs mainly on the surface and deeper parts of the carbon material remain non-functionalized. Carbon remains dominant, confirming that the SPCE's structural integrity is preserved despite surface modifications. The gradual reduction of Cl content with increased time of plasma treatment suggests its removal, which is in line with XPS data.

3.1.3. FTIR/ATR

FTIR ATR spectra for all samples are shown in Fig. 3. The pristine SPCE spectrum reveals sharp and well-defined bands in the 700–1200 cm^{-1} region, which are attributed to C–O stretching vibrations from aliphatic ethers, phenols, and epoxy groups [37]. Sample 1 SPCE, 3 SPCE and 5 SPCE exhibit similar bands in this region, indicating the presence of diverse and overlapping oxygenated functionalities [38].

In the 1600–1750 cm^{-1} region, a sharp band near 1700 cm^{-1} observed in all the samples corresponds to the C=O vibrations. In the 2300–2400 cm^{-1} region, a weak band appears across all samples, due to the asymmetric stretching of atmospheric CO_2 (O=C=O). Although not associated with specific surface functionalities, its presence is common in ATR spectra measured under ambient conditions. The 2900–3000 cm^{-1}

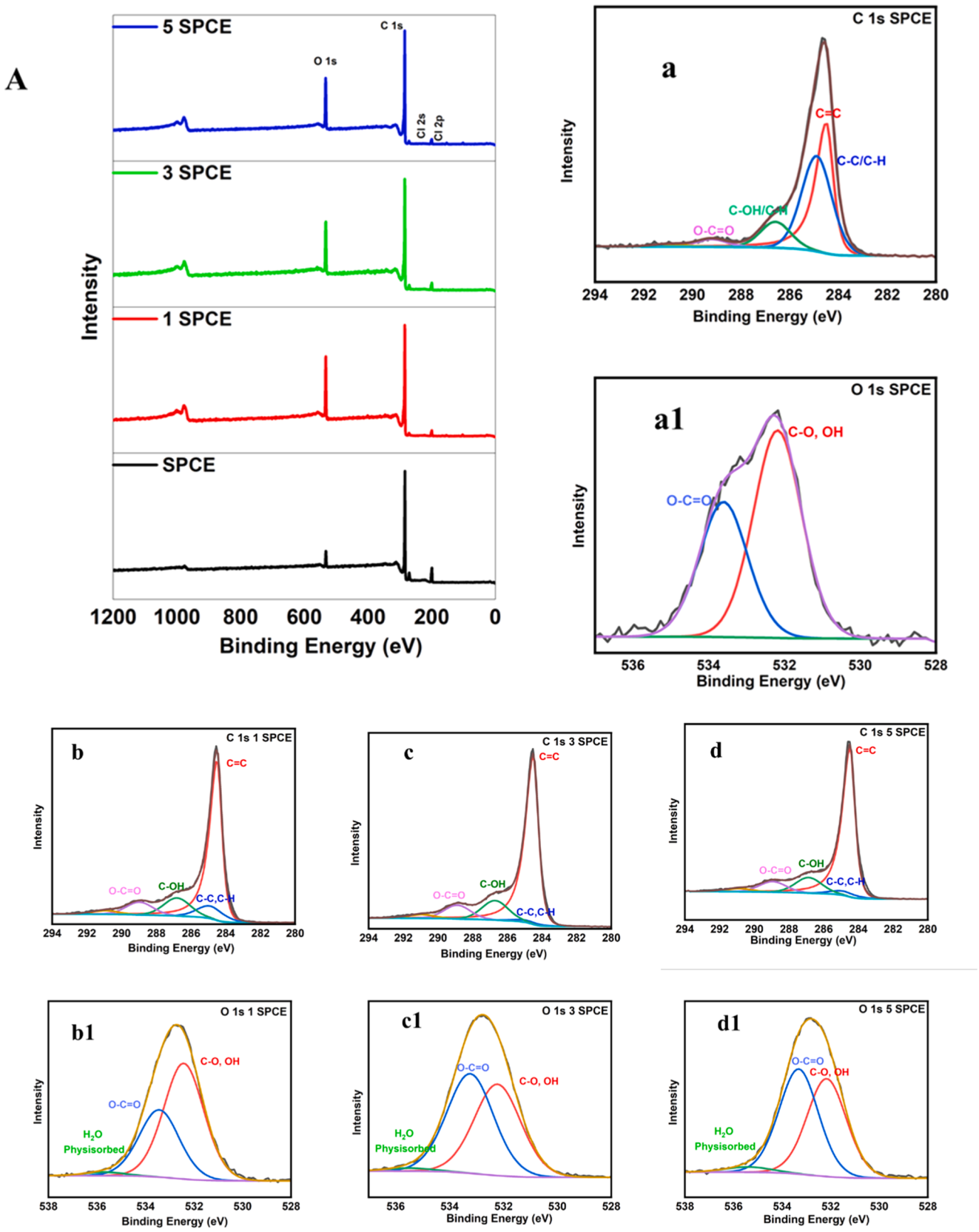

Fig. 2. A) XPS survey scan of the electrodes before (SPCE) and after plasma treatment (1 SPCE, 3 SPCE and 5 SPCE). High-resolution C 1s spectrum of the pristine SPCE (a), 1 SPCE (b), 3 SPCE (c) and 5 SPCE (d). High-resolution O 1s spectrum of the pristine SPCE (a1), 1 SPCE (b1), 3 SPCE (c1) and 5 SPCE (d1).

Table 1
Elemental composition of the samples analysed by XPS.

Sample Element	SPCE		1 SPCE		3 SPCE		5 SPCE	
	Position	%At Conc. ±SD	Position	%At Conc. ±SD	Position	%At Conc. ±SD	Position	%At Conc. ±SD
O 1s	532.34	5.18±0.23	532.61	13.96±0.23	532.58	12.28±0.26	532.75	12.68 ± 0.20
C 1s	284.50	89.80±0.26	284.50	84.71±0.26	284.50	85.93±0.28	284.50	83.99 ± 0.24
Cl 2p	200.01	5.02±0.11	200.12	1.33±0.05	199.95	1.79±0.08	199.75	1.91 ± 0.06

Table 2
XPS data analysis of the C 1s and O 1s peaks.

Sample Moiety		SPCE		1 SPCE		3 SPCE		5 SPCE	
		Position	%At Conc	Position	%At Conc	Position	%At Conc	Position	%At Conc
C 1s	C=C	284.50	61.16	284.50	91.33	284.50	91.88	284.44	74.00
	C-C, C-H	284.90	28.94	284.89	1.22	284.89	0.38	284.84	3.32
	C-OH	286.56	7.69	286.88	4.02	286.80	4.09	286.80	12.28
	O-C=O	289.07	1.83	289.15	2.96	289.15	3.00	288.92	8.33
	pi-pi*	290.93	0.39	290.93	0.46	290.93	0.64	290.87	2.06
O 1s	C-O, -OH	532.24	61.70	532.40	57.80	532.35	53.76	532.09	47.20
	O-C=O	533.60	38.30	533.45	39.84	533.36	44.31	533.25	49.37
	H_2O adsorbed	–	–	535.28	2.36	535.61	1.93	535.39	3.43

Table 3

Sample Element	SPCE %At Conc. ±SD	1 SPCE %At Conc. ±SD	3 SPCE %At Conc. ±SD	5 SPCE %At Conc. ±SD
O	2.32±0.79	2.91±2.89	3.20±0.96	3.23 ± 0.93
C	94.47±10.91	94.21±10.69	94.06±10.75	93.91 ± 10.60
Cl	3.22±0.33	2.89±0.30	2.75±0.29	2.68± 0.29

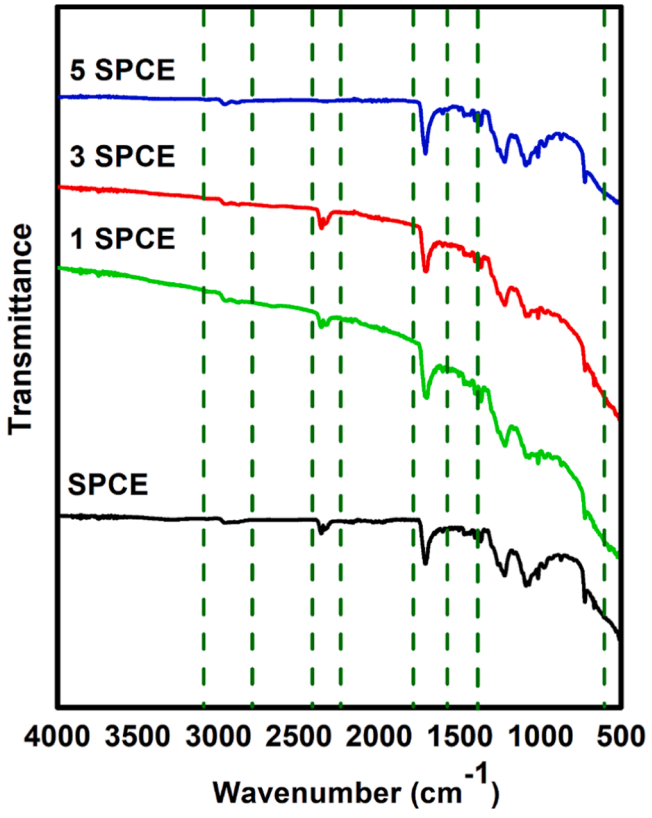

Fig. 3. FTIR ATR spectra of SPCE, 1 SPCE, 3 SPCE and 5 SPCE.

region features low-intensity bands, corresponding to asymmetric and symmetric C–H stretching, indicating the chemisorption of hydrogen on the graphitic surface [39]. The small differences observed in the FTIR spectra of pristine and modified samples may be due to the fact that FTIR measures the bulk of the material rather than being surface-specific. Since infrared radiation can penetrate into the sample, any surface modifications may not be strongly reflected in the spectrum if the bulk composition remains largely unchanged (surface-only changes may have minimal impact on the overall spectrum). This interpretation is consistent with the EDX results, which also probe beyond just the surface and showed minimal variation in C/O ratio.

3.1.4. Contact angle

Contact angle measurements were conducted to evaluate the wettability changes in the SPCE surfaces upon plasma treatment. As shown in Fig. 4, the pristine SPCE displayed a high average contact angle of ~124±5°, indicating a hydrophobic surface. This hydrophobic nature corresponds well with the XPS results, which revealed the dominant presence of graphitic carbon (C=C) and surface hydrocarbons (C–C/

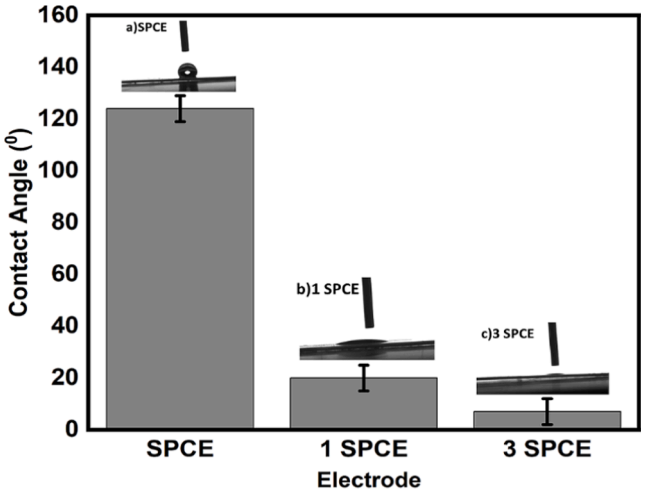

Fig. 4. Contact angle measurements of the SPCE, 1 SPCE, and 3 SPCE. The bar chart shows the change in surface wettability with standard deviation. Insets display representative water droplet images of (a) SPCE, (b) 1 SPCE, and (c) 3 SPCE, highlighting the transition from hydrophobic to hydrophilic surface after plasma treatment.

C–H), as well as limited surface oxygen functionalities. The FTIR-ATR spectra also revealed strong peaks in the 2900–3000 cm^{-1} region (C–H stretching), confirming the presence of aliphatic hydrocarbons that contribute to the hydrophobic character. In the case of 1 SPCE, the contact angle dropped significantly to an average of ~20°±5° and further decreased to ~7°±5° for 3 SPCE, clearly demonstrating a transition to a hydrophilic surface. This transition is attributed to the introduction of oxygen-containing polar groups (–OH, –COOH), as evidenced by XPS O 1 s deconvolution and the appearance of broad O–H and C=O features in the FTIR region between 1600–1750 cm^{-1} and 700–1200 cm^{-1}. Notably, ten measurements were taken consecutively on the same electrode at different points to assess reproducibility and surface uniformity. These findings, in correlation with the XPS and FTIR data, confirm that oxygen plasma treatment effectively cleans and functionalizes the SPCE surface, significantly enhancing its wettability, which can improve the electrochemical performance due to increased surface reactivity. Sample 5 SPCE exhibited complete wetting behavior, characterized by a contact angle of approximately 0° Upon deposition, the water droplet did not retain a defined shape but spread instantly across the surface to form a continuous thin film. This indicates a highly hydrophilic surface with strong adhesive interactions between the water and the substrate.

3.2. Electrochemical properties of the pre- and post-treated electrodes

3.2.1. Cyclic voltammetry (CV)

CV was employed to investigate the electrochemical behavior and redox kinetics of the screen-printed carbon electrode (SPCE) before and after plasma treatment. Measurements were carried out using a 40 mM $[Fe(CN)_6]^{3-/4-}$ redox couple in a 0.1 M KCl electrolyte, with scan rates ranging from 10 to 150 mV/s. The selected concentration was chosen to ensure a strong electrochemical response from the electrode while remaining within its linear detection range (see Fig. S4). Although higher redox probe concentrations may raise concerns about non-ideal diffusion or ion pairing [40], no such effects were observed within the tested range. As shown in Fig. 5a–d, the untreated SPCE exhibited the lowest anodic and cathodic peak currents, indicative of a limited electroactive surface area and slower electron transfer. In contrast, the plasma-treated electrodes (1 SPCE, 3 SPCE, and 5 SPCE) presented consistent and marked increases in both the anodic and cathodic peak currents with increasing scan rates (Fig. 5b–d). This enhancement is attributed to surface activation via oxygen plasma, which introduces oxygen-containing functional groups (e.g., –OH and –COOH) and modifies the surface morphology, as supported by FTIR (Fig. 3) and XPS analysis (Fig. 2). These chemical modifications increase surface hydrophilicity and wettability (discussed in Section 3.1.4), facilitating better accessibility of redox species to the electrode surface. To further analyse the kinetics of the redox reaction, the dependence of the peak current (Ip) on the square root of the scan rate ($\nu^{1/2}$) was examined (Fig. 5e). The linear relationship observed for all electrodes confirms that the electron transfer process is diffusion-controlled, which is consistent with the Randles–Sevcik equation **Eq**. (3.2.1) for an irreversible system [41],

$$\boldsymbol{Ip} = \left(2.99 \times 10^5\right)\boldsymbol{n}^{3/2}\boldsymbol{AD}^{1/2}\boldsymbol{C}\boldsymbol{\nu}^{1/2}\ \boldsymbol{\alpha}^{1/2} \quad (3.2.1)$$

where

I p is the peak current (A),
n is the number of electrons transferred (n = 1 for the ferro/ferri system),
A is the electroactive surface area (cm^2), used as an ECSA
D is the diffusion coefficient (~7.6×10^{-6} cm^2/s for $[Fe(CN)_6]^{3-/4-}$),
C is the concentration (mol/cm^3),
ν is the scan rate (V/s)
α = charge transfer coefficient (dimensionless, α =0.3, determined according to [41])

In a truly reversible electrochemical redox reaction, the separation between the anodic and cathodic peaks (ΔEp) is approximately 59.2 mV divided by the number of electrons transferred. The studied systems show irreversible redox behaviour based on ΔEp values >59 mV, as can be seen in Fig. 5 a-d. However, linearity of $I = f(\nu^{1/2})$ proves, that Randles-Sevcic equation can be used to describe the redox behaviour of

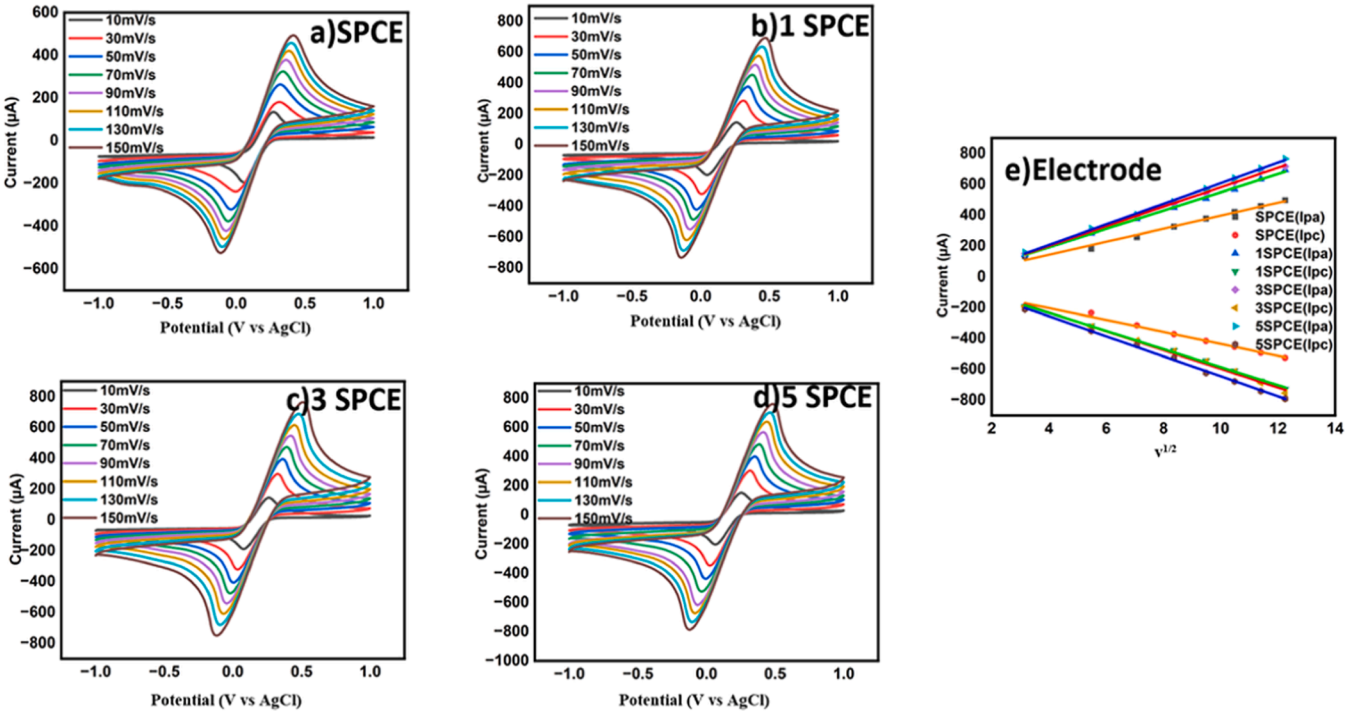

Fig. 5. Cyclic voltammetry curves of (a) SPCE, (b) 1 SPCE, (c) 3 SPCE, and (d) 5 SPCE recorded in 40 mM $[Fe(CN)_6]^{3-/4-}$ solution containing 0.1 M KCl at scan rates ranging from 10 to 150 mV/s. (e) Corresponding anodic and cathodic peak current vs. square root of the scan rate plot showing diffusion-controlled kinetics.

the studied system on pristine and functionalized SPCE with good approximation. Based on this assumption, using the above Eq. (3.2.1) and the slope of the I_p vs. $\nu^{1/2}$ plot, the electrochemical active surface area (ECSA) was calculated. The calculated approximate areas increased from 0.069 cm^2 for SPCE to 0.096 cm^2 for 1 SPCE, 0.102 cm^2 for 3 SPCE, and 0.106 cm^2 for 5 SPCE, demonstrating a significant increase in the electrochemical surface area upon plasma treatment.

3.2.2. Electrochemical impedance spectroscopy (EIS)

EIS was employed to study the interfacial electron transfer behavior of the bare and plasma-modified screen-printed carbon electrodes (SPCEs). The measurements were carried out in a frequency range of 100 mHz to 100 kHz with an AC amplitude of 10 mV. The Nyquist plots (Fig. 6A) were analyzed using the Randles equivalent circuit model, which includes a solution resistance (Rs), charge transfer resistance (R_{ct}), constant phase element (CPE), and Warburg impedance (W), accounting for both kinetic and diffusion-controlled processes. The Rs remained nearly constant at around 300±15 Ω for all electrodes, indicating consistent electrolyte conditions. However, a significant difference in Rct was observed: the bare SPCE exhibited a high Rct of 2606 ±10 Ω, suggesting limited electron transfer due to its hydrophobic and less conductive surface. This is typical for untreated carbon surfaces, which generally show sluggish kinetics of redox reactions due to limited surface functionality and lower ECSA.

After plasma treatment, the electrodes (1 SPCE, 3 SPCE, and 5 SPCE) showed a dramatic decrease in R_{ct}, with values dropping to 33.4±0.5 Ω, 3.2±0.2 Ω, and 2.1±0.1 Ω, respectively. This improvement is attributed to the surface activation and functionalization induced by plasma exposure, which enhances surface wettability and introduces oxygen-containing functional groups, thereby facilitating faster electron transfer. These findings were supported by corresponding increases in ECSA, estimated using the Randles–Sevcik equation from cyclic voltammetry data **Eq**. (3.2.1).

To quantify the electron transfer efficiency, the heterogeneous electron transfer rate constant (k_{et}) was estimated ***Eq***. (3.2.2)using a modified form of the Randles–Sevcik equation based on EIS data:

$$k_{et} = \frac{RT}{n^2F^2ACR_{ct}} \quad (3.2.2)$$

Where:

- R = 8.314 J mol^{-1} K^{-1} (gas constant),
- T = 298 K (room temperature),
- n = 1 (number of electrons transferred),
- F = 96,485 C mol^{-1} (Faraday constant),
- A = electrochemically active surface area (calculated from CV),
- C = 0.04 mol L^{-1} (40 mM redox species),
- R_{ct} = charge transfer resistance (from Nyquist plots).

Using the electrochemically active surface area (ECSA) values determined from cyclic voltammetry - 0.069 cm^2 for SPCE to 0.096 cm^2 for 1 SPCE, 0.102 cm^2 for 3 SPCE, and 0.106 cm^2 for 5 SPCE, the corresponding heterogeneous electron transfer rate constants (k_{et}) were calculated as approximately 3.70 × 10^{-7} cm/s, 2.08 × 10^{-5} cm/s, 2.06 × 10^{-4} cm/s, and 2.99 × 10^{-4} cm/s, respectively. These values clearly indicate a marked improvement in charge transfer kinetics as a result of plasma treatment. This enhancement is attributed to plasma-induced modifications, including increased surface roughness and porosity, the incorporation of oxygen-containing functional groups, and improved surface wettability-all of which contribute to a greater electrochemical active area and more efficient interfacial electron transfer.

The enhanced performance of modified electrodes is thus a combined effect of increased active surface area (due to increased porosity) and improved surface conductivity. These modifications significantly improve the kinetics of the redox reaction, making the modified SPCEs highly suitable for electrochemical sensing applications

4. Correlation analysis of surface and electrochemical parameters

To explore the synergy between wettability and electrochemical kinetics, we propose a performance model where ECSA and ket are related to the R_{ct} and the cosine of the contact angle (cos(θ)). This model suggests that oxygen plasma treatment improves both electrode-electrolyte interaction and charge transport properties by modifying the surface morphology and enhancing the wettability of the electrode. Specifically, plasma-treated SPCEs demonstrated a remarkable reduction in R_{ct} by a factor of 1000, indicating improved charge transfer kinetics, and a more than 10-fold increase in ECSA, highlighting an enhanced surface area for electrochemical reactions. The pristine SPCE (with a contact angle of 124° and R_{ct} of 2606 Ω) exhibited the lowest ECSA (~0.069 cm^2 and the lowest k_{et} (~3.70 × 10^{-7} cm/s) (Fig. 7). In contrast, the 1 SPCE (contact angle = 20°, R_{ct} = 33.4 Ω), 3 SPCE (contact angle = 7°, R_{ct} = 3.17 Ω), and 5 SPCE (contact angle = 5°, R_{ct} = 2.1 Ω) progressive enhancement in electrochemical performance, with the electroactive surface area increasing from 0.069 cm^2 for SPCE to 0.096 cm^2 for 1 SPCE, 0.102 cm^2 for 3 SPCE, and 0.106 cm^2 for 5 SPCE. Correspondingly, the heterogeneous electron transfer rate constants (k_{et}) were estimated to be approximately 3.70 × 10^{-7} cm/s, 2.08 × 10^{-5} cm/s, 2.06 × 10^{-4} cm/s, and 2.99 × 10^{-4} cm/s, respectively. Fig. 7).

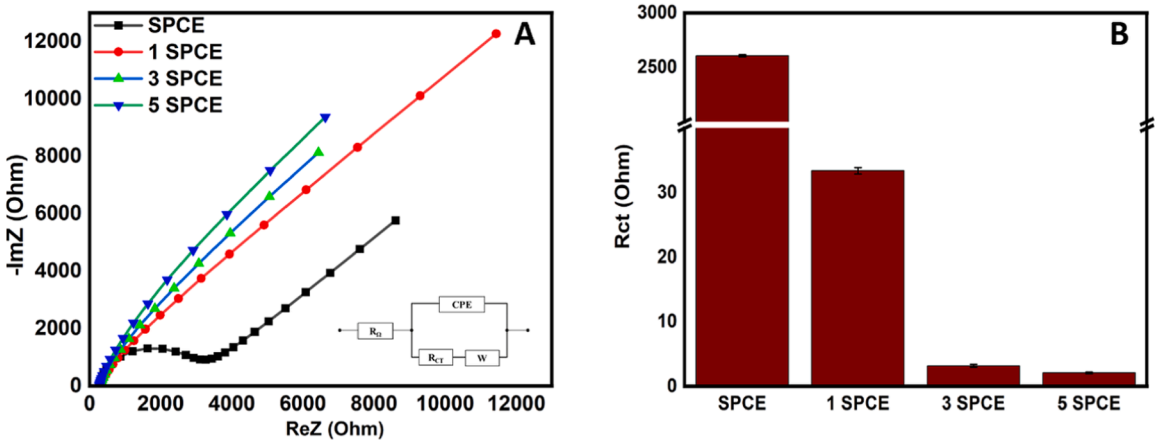

Fig. 6. (A) Nyquist plots of the fitted EIS data for SPCE, 1 SPCE, 3 SPCE, and 5 SPCE electrodes recorded in 40 mM $[Fe(CN)_6]^{3-/4-}$ solution; inset shows the equivalent Randles circuit used for fitting. (B) Bar diagram illustrating the charge transfer resistance (Rct) values for each electrode; 3 SPCE and 5 SPCE to emphasize the significant reduction in Rct after plasma treatment.

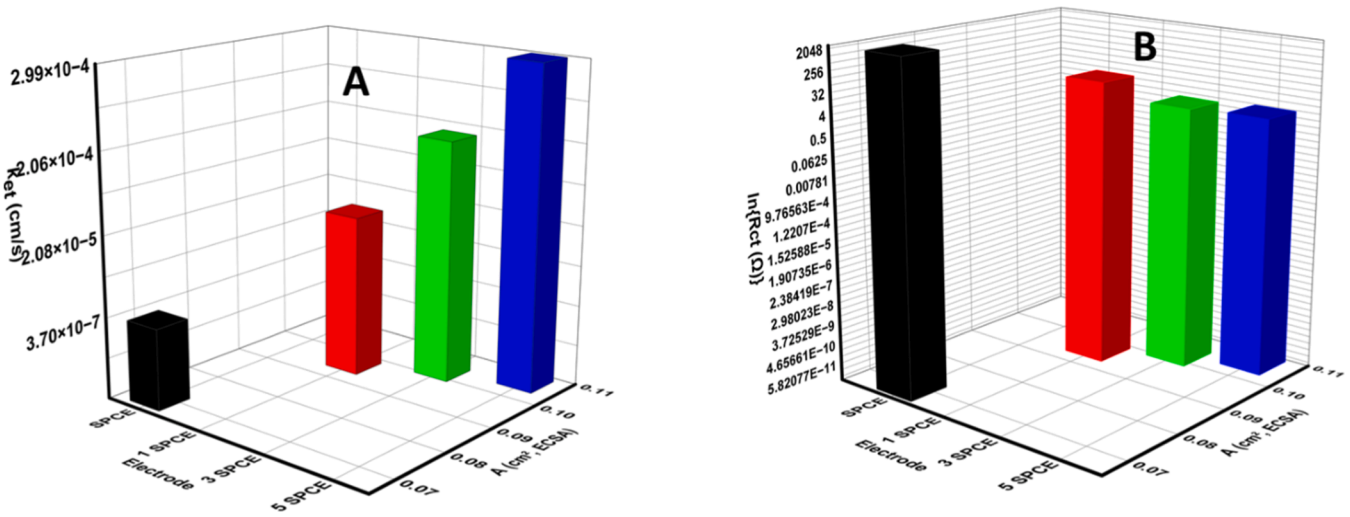

Fig. 7. A) shows 3D bar plots comparing the electrochemical performance of SPCE, 1 SPC E, 3 SPCE, and 5 SPCE electrodes, highlighting a significant increase in ECSA and an enhancement in electron transfer rate constant (ket) with increasing plasma treatment cycles. B) illustrates a marked decrease in charge transfer resistance (R_{ct})-presented on a logarithmic scale-further confirming improved electrode kinetics. In both cases, the ECSA consistently increases with successive plasma treatments.

Based on these observations, the following empirical relationships are proposed to quantitatively describe the electrochemical performance of the plasma-treated electrodes:

$$\boldsymbol{ECSA} = \boldsymbol{k}_1.\frac{\cos(\boldsymbol{\theta})}{\boldsymbol{R}_{ct}},\ \boldsymbol{k}_{et} = \boldsymbol{k}_2.\frac{\cos(\boldsymbol{\theta})}{\boldsymbol{R}_{ct}} \tag{4.1}$$

In these equations, k_1 reflects the effectiveness of surface wettability in promoting electrochemical accessibility. It quantifies how efficiently a given increase in cos(θ) translates into an increased ECSA. Higher values of k_1 suggest a more porous, roughened, or chemically functionalized surface that takes greater advantage of improved wettability. k_2 represents the intrinsic electronic and electrochemical properties of the electrode material that influence charge transfer at the interface. It is governed by factors such as surface conductivity, availability of reactive sites, and the density of states. A higher k_2 value indicates more efficient charge transport mechanisms inherent to the electrode architecture. This model provides a robust framework for optimizing plasma treatment conditions, which can be tailored to fabricate high-performance electrochemical sensors. The relationship highlights the importance of surface modification for improving sensor efficiency, particularly for applications in biosensing, energy storage, and electrocatalysis.

5. Repeatability and stability

To evaluate the repeatability and stability of the plasma-treated electrodes, CV measurements were performed using SPCE, 1 SPCE, 3 SPCE, and 5 SPCE electrodes. Repeatability was assessed by performing five consecutive CV scans for each electrode under identical conditions. The corresponding bar diagram representing the anodic and cathodic peak currents (Fig. 8A) demonstrates excellent reproducibility, with a standard deviation (n = 5) of less than 3 % for all electrodes. This confirms the robustness of the redox behavior and the consistent surface activity of the electrodes. The associated cyclic voltammograms supporting these findings are provided in Supplementary Fig. S5, which shows overlapping curves with negligible deviation across cycles. For the stability study, electrodes were stored under ambient conditions (room temperature, 20 ± 3°C) and tested at six days intervals: 0, 1, 3, 5, 7, and 20 days. Each sample was analyzed in triplicate (n = 3) to ensure statistical reliability. The stability data are illustrated in Fig. 8B, which presents the bar diagram of anodic and cathodic currents over time. The corresponding CVs are shown in Supplementary Fig. S6. Plasma-treated electrodes particularly 3 SPCE and 5 SPCE exhibited significantly greater retention of redox current over the 20-day period, with minimal degradation compared to the pristine SPCE, which showed a noticeable

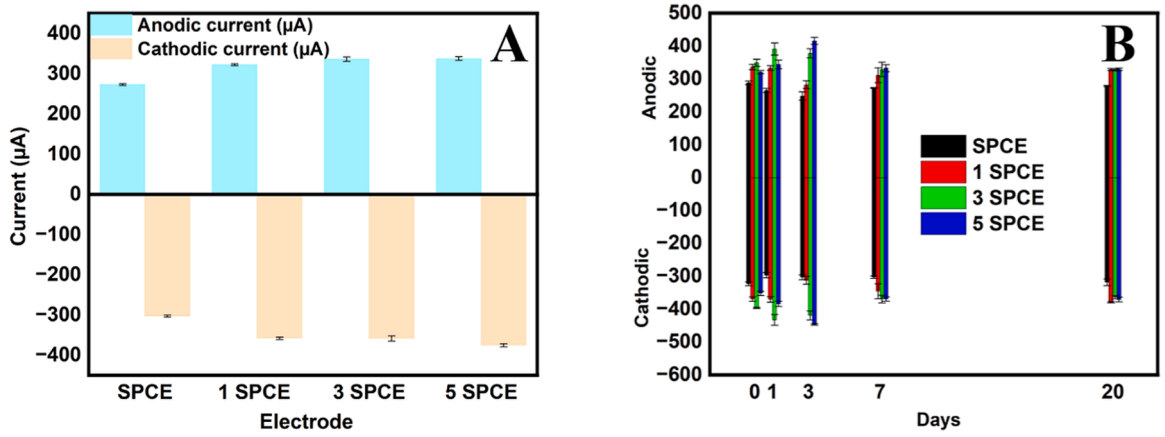

Fig. 8. A) Repeatability of SPCE, 1 SPCE, 3 SPCE, and 5 SPCE electrodes showing anodic and cathodic peak currents with <3 % standard deviation (n = 5). B) Stability of electrodes over 20 days under ambient conditions (n = 3), indicating minimal degradation in plasma-treated electrodes.

decline in both cathodic and anodic responses. The small error bars across time points reflect high consistency and support the effectiveness of plasma treatment in enhancing surface stability.

6. Conclusion

In this study, we presented a simple and scalable oxygen plasma treatment strategy that markedly improved the electrochemical performance of screen-printed carbon electrodes (SPCEs). Surface analysis confirmed the successful incorporation of oxygen-containing functional groups, which significantly enhanced the electrodes' wettability and polar groups. Contact angle measurements revealed a clear shift from hydrophobic to hydrophilic behaviour, highlighting improved interactions at the electrode–electrolyte interface. Electrochemical characterization demonstrated a substantial increase in the ECSA and enhanced redox kinetics with increasing plasma exposure. CV, particularly scan-rate-dependent studies, confirmed a diffusion-controlled process through the linearity between the peak current and the square root of the scan rate. EIS further validated these enhancements, with Rct dramatically decreasing from approximately 2600 Ω in pristine SPCEs to as low as 2 Ω in plasma-treated variants by a factor of 1000. Correspondingly, the ket significantly increased, indicating improved charge transfer efficiency. To capture the synergistic effect of wettability and electrochemical performance, we proposed a predictive model where both ECSA and ket scale proportionally with the cosine of the contact angle (cos θ) and inversely with R_{ct}. This model provides a quantitative basis for optimizing plasma treatment parameters to fine-tune electrode performance. To ensure the stability and repeatability of the electrodes, both pristine and plasma-treated SPCEs were evaluated. The plasma-treated electrodes demonstrated superior reproducibility (n = 5) and minimal degradation over time, confirming enhanced electrochemical stability. Collectively, these findings underscore the potential of plasma surface engineering as a powerful tool for developing high-performance, cost-effective, and disposable electrochemical platforms, with promising applications in biosensing, energy conversion, and environmental monitoring.

CRediT authorship contribution statement

Sunil Luhar: Writing – original draft, Methodology, Investigation, Data curation, Conceptualization. **Kamila Sadowska:** Writing – review & editing, Supervision, Funding acquisition, Conceptualization.

Declaration of competing interest

The authors declare the following financial interests/personal relationships which may be considered as potential competing interests: Kamila Sadowska reports financial support was provided by National Science Centre Poland. If there are other authors, they declare that they have no known competing financial interests or personal relationships that could have appeared to influence the work reported in this paper.

Acknowledgements

The authors gratefully acknowledge the financial support provided by the National Science Centre (Project No. 2023/50/E/ST5/00347). The authors also sincerely thank the ENSEMBLE^3 Centre of Excellence (Wolczynska 133, Warsaw 01–919, Poland) for facilitating the AFM measurements. Special thanks are extended to Dr. Kingshuk Bandopadhyay and Dr. Pradip Kumar Roy for their assistance with the AFM analysis.

Supplementary materials

Supplementary material associated with this article can be found, in the online version, at doi:10.1016/j.surfin.2025.107943.

Data availability

The data that supports the findings of this study are available from the corresponding author on request.

References

[1] C. Chen, Y. Fu, Y. Liu, P. Dutta, Y. Lin, D. Du, K. Qiu, Next-generation health monitoring: The role of nanomaterials in 3D-printed wearable devices, Mater. Today 86 (2025) 317–339, https://doi.org/10.1016/J.MATTOD.2025.03.005.
[2] H.D. Yoo, E. Markevich, G. Salitra, D. Sharon, D. Aurbach, On the challenge of developing advanced technologies for electrochemical energy storage and conversion, Mater. Today 17 (2014) 110–121, https://doi.org/10.1016/J.MATTOD.2014.02.014.
[3] S. Luhar, R. Ghosh, P.B. Chatterjee, D.N. Srivastava, An impedometric sensor based on boronic acid @ plastic chip electrode for sensitive detection of prostate cancer biomarker spermine, Biosens. Bioelectron. X 12 (2022) 100219, https://doi.org/10.1016/j.biosx.2022.100219.
[4] T. Sakthi Priya, T.W. Chen, S.M. Chen, T. Kokulnathan, B.S. Lou, T. saad Algarni, W.A. Al-onazi, M.S. Elshikh, MIL-88A derived zerovalent iron embedded mesoporous carbon with carbon black composite based electrochemical sensor for the detection of metol, Carbon N Y 223 (2024) 119026, https://doi.org/10.1016/J.CARBON.2024.119026.
[5] K.B. Patel, S. Luhar, D.N. Srivastava, Plastic chip electrode: an emerging multipurpose electrode platform, Chem. Asian J. 18 (2023) e202300690, https://doi.org/10.1002/asia.202300690.
[6] A. Dettlaff, M. Sobaszek, T. Klimczuk, R. Bogdanowicz, Enhanced electrochemical kinetics of highly-oriented (111)-textured boron-doped diamond electrodes induced by deuterium plasma chemistry, Carbon N Y 174 (2021) 594–604, https://doi.org/10.1016/J.CARBON.2020.11.096.
[7] J. Miao, T. Fan, Flexible and stretchable transparent conductive graphene-based electrodes for emerging wearable electronics, Carbon N Y 202 (2023) 495–527, https://doi.org/10.1016/J.CARBON.2022.11.018.
[8] M. Li, Y.T. Li, D.W. Li, Y.T. Long, Recent developments and applications of screen-printed electrodes in environmental assays—a review, Anal. Chim. Acta 734 (2012) 31–44, https://doi.org/10.1016/J.ACA.2012.05.018.
[9] Z. Yang, T. Guo, Q. Hu, J. Liu, X. Chen, Y. Wang, L.M. Liu, Z. Wang, L. Guo, How amorphous CoOx(OH)y-Pd nanocomposite endows high performance and durability in methanol oxidation reaction, Mater. Today 86 (2025) 255–266, https://doi.org/10.1016/J.MATTOD.2025.03.032.
[10] J. Si, H. Lan, J. An, S. Ge, W. Liu, Y.M. Zhang, X. Mao, W. He, Emerging reactive oxygen and nitrogen species regulators for biomedical therapy: 2D MXenzymes, Mater. Today 85 (2025) 112–140, https://doi.org/10.1016/J.MATTOD.2025.02.004.
[11] L. Sasso, S. Suei, L. Domigan, J. Healy, V. Nock, M.A.K. Williams, J.A. Gerrard, Versatile multi-functionalization of protein nanofibrils for biosensor applications, Nanoscale 6 (2014) 1629–1634, https://doi.org/10.1039/c3nr05752f.
[12] I. Mazurenko, V.P. Hitaishi, E. Lojou, Recent advances in surface chemistry of electrodes to promote direct enzymatic bioelectrocatalysis, Curr. Opin. Electrochem. 19 (2020) 113–121, https://doi.org/10.1016/j.coelec.2019.11.004.
[13] F. Figueredo, M.J. González-Pabón, E. Cortón, Low cost layer by layer construction of CNT/chitosan flexible paper-based electrodes: a versatile electrochemical platform for point of care and point of need testing, Electroanalysis 30 (2018) 497–508, https://doi.org/10.1002/elan.201700782.
[14] J.Z. Tsai, C.J. Chen, K. Settu, Y.F. Lin, C.L. Chen, J.T. Liu, Screen-printed carbon electrode-based electrochemical immunosensor for rapid detection of microalbuminuria, Biosens. Bioelectron. 77 (2016) 1175–1182, https://doi.org/10.1016/J.BIOS.2015.11.002.
[15] K.F. Chan, H.N. Lim, N. Shams, S. Jayabal, A. Pandikumar, N.M. Huang, Fabrication of graphene/gold-modified screen-printed electrode for detection of carcinoembryonic antigen, Mater. Sci. Eng. C 58 (2016) 666–674, https://doi.org/10.1016/J.MSEC.2015.09.010.
[16] C. Corbella, A. Aijaz, T. Kubart, L. Lin, S. Portal, M. Keidar, Pulsed plasma vapour deposition of carbon materials: Advantages and challenges, Carbon N Y 232 (2025) 119772, https://doi.org/10.1016/J.CARBON.2024.119772.
[17] C.M. Seah, B. Vigolo, S.P. Chai, A.R. Mohamed, Mechanisms of graphene fabrication through plasma-induced layer-by-layer thinning, Carbon N Y 105 (2016) 496–509, https://doi.org/10.1016/J.CARBON.2016.04.072.
[18] Z. Chen, G. Chen, R. Obenchain, R. Zhang, F. Bai, T. Fang, H. Wang, Y. Lu, R. E. Wirz, Z. Gu, Cold atmospheric plasma delivery for biomedical applications, Mater. Today 54 (2022) 153–188, https://doi.org/10.1016/J.MATTOD.2022.03.001.
[19] A.S. Elewi, S.A.W. Al-Shammaree, A.K.M.A. AL Sammarraie, Hydrogen peroxide biosensor based on hemoglobin-modified gold nanoparticles–screen printed carbon electrode, Sens. Biosensing. Res. 28 (2020) 100340, https://doi.org/10.1016/j.sbsr.2020.100340.
[20] A. Roberts, H. Dhanze, G.T. Sharma, S. Gandhi, Point-of-care detection of Japanese encephalitis virus biomarker in clinical samples using a portable smartphone-enabled electrochemical "Sensit" device, Bioeng. Transl. Med. 8 (2023) e10506, https://doi.org/10.1002/btm2.10506.
[21] M. Karthikeyan, M. Dhinesh Kumar, G. Kaniraja, P. Ananthappan, V. Sivasamy Vasantha, C. Karunakaran, Gold nanoparticles enhanced molecularly imprinted poly(3-aminophenylboronic acid) sensor for myo-inositol detection, Microchem. J. 189 (2023) 108536, https://doi.org/10.1016/j.microc.2023.108536.

[22] R. Jiménez-Pérez, M.I. González-Sánchez, A. Gomis-Berenguer, J. Iniesta, E. Valero, Enhanced surface properties and electrochemical performance of carbon-based screen-printed electrodes via hydrogen peroxide activation, Electrochim. Acta 536 (2025) 146721, https://doi.org/10.1016/J.ELECTACTA.2025.146721.
[23] L. Wen, J. Wang, Z. Liu, C.A. Tao, J. Rao, J. Hang, Y. Li, A portable acetylcholinesterase-based electrochemical sensor for field detection of organophosphorus, RSC Adv. 13 (2023) 6389–6395, https://doi.org/10.1039/d2ra05383g.
[24] Z. Zhang, J.L. Wilson, B.R. Kitt, D.W. Flaherty, Effects of oxygen plasma treatments on surface functional groups and shear strength of carbon fiber composites, ACS Appl Polym. Mater. 3 (2021) 986–995, https://doi.org/10.1021/acsapm.0c01270.
[25] S. Luhar, R. Rane, D.N. Srivastava, Surface tailored graphite–polymer composite electrodes through cold plasma for electrochemical applications, Plasma Process. Polym. 19 (2022) 2200048, https://doi.org/10.1002/ppap.202200048.
[26] K. Barman, S. Luhar, R. Rane, D.N. Srivastava, S.K. Nema, S. Bhattacharjee, Improving electrochemical sensitivity of screen-printed carbon electrodes by atmospheric pressure plasma jet treatment and electrochemical detection of dopamine, Plasma Process. Polym. 20 (2023) 2200161, https://doi.org/10.1002/ppap.202200161.
[27] E.C. Neyts, K. Ostrikov, M.K. Sunkara, A. Bogaerts, Plasma catalysis: synergistic effects at the nanoscale, Chem. Rev. 115 (2015) 13408–13446, https://doi.org/10.1021/acs.chemrev.5b00362.
[28] F. Khelifa, S. Ershov, Y. Habibi, R. Snyders, P. Dubois, Free-radical-induced grafting from plasma polymer surfaces, Chem. Rev. 116 (2016) 3975–4005, https://doi.org/10.1021/acs.chemrev.5b00634.
[29] A.I. Aria, B.J. Lyon, M. Gharib, Morphology engineering of hollow carbon nanotube pillars by oxygen plasma treatment, Carbon N Y 81 (2015) 376–387, https://doi.org/10.1016/J.CARBON.2014.09.070.
[30] X. Yuan, L. Ma, J. Zhang, Y. Zheng, Simple pre-treatment by low-level oxygen plasma activates screen-printed carbon electrode: Potential for mass production, Appl. Surf. Sci. 544 (2021) 148760, https://doi.org/10.1016/J.APSUSC.2020.148760.
[31] J.P. Boudou, J.I. Paredes, A. Cuesta, A. Martínez-Alonso, J.M.D. Tascón, Oxygen plasma modification of pitch-based isotropic carbon fibres, Carbon N Y 41 (2003) 41–56, https://doi.org/10.1016/S0008-6223(02)00270-1.
[32] S.C. Wang, K.S. Chang, C.J. Yuan, Enhancement of electrochemical properties of screen-printed carbon electrodes by oxygen plasma treatment, Electrochim. Acta 54 (2009) 4937–4943, https://doi.org/10.1016/J.ELECTACTA.2009.04.006.
[33] J.Y. Lee, E.J. Park, C.J. Lee, S.W. Kim, J.J. Pak, N.K. Min, Flexible electrochemical biosensors based on O2 plasma functionalized MWCNT, Thin Solid Films 517 (2009) 3883–3887, https://doi.org/10.1016/J.TSF.2009.01.130.
[34] K.Z. Donato, G.K.W. Koon, S.J. Lee, A. Carvalho, H.L. Tan, M.C.F. Costa, J. Tolasz, P. Ecorchard, P.P. Michałowski, R.K. Donato, A.H. Castro Neto, Disordered metallic carbon materials from graphene edge chemistry, Mater. Today 79 (2024) 49–59, https://doi.org/10.1016/J.MATTOD.2024.07.011.
[35] P. Stelmachowski, D. Maj, G. Grzybek, K. Kruczała, A. Kotarba, Functionalization of Graphite with Oxidative Plasma, Int. J. Mol. Sci. 23 (17) (2022 Aug 5) 9650, https://doi.org/10.3390/ijms23179650.
[36] I. Kondratowicz, M. Nadolska, S. Şahin, M. Łapiński, M. Prześniak-Welenc, M. Sawczak, E.H. Yu, W. Sadowski, K. Żelechowska, Tailoring properties of reduced graphene oxide by oxygen plasma treatment, Appl. Surf. Sci. 440 (2018) 651–659, https://doi.org/10.1016/J.APSUSC.2018.01.168.
[37] M.B. Hay, S.C.B. Myneni, Structural environments of carboxyl groups in natural organic molecules from terrestrial systems. Part 1: Infrared spectroscopy, Geochim. Cosmochim. Acta 71 (2007) 3518–3532, https://doi.org/10.1016/J.GCA.2007.03.038.
[38] X. Liu, P. Zhao, F. Liu, R. Lin, H. Yao, S. Zhu, Attenuated total reflection infrared spectroscopy for studying electrochemical cycling of hydrogen, carbon, and nitrogen-containing molecules, J. Energy Chem. 99 (2024) 495–511, https://doi.org/10.1016/J.JECHEM.2024.08.008.
[39] H. Wang, Y.W. Zhou, W.B. Cai, Recent applications of in situ ATR-IR spectroscopy in interfacial electrochemistry, Curr. Opin. Electrochem. 1 (2017) 73–79, https://doi.org/10.1016/J.COELEC.2017.01.008.
[40] C. Batchelor-McAuley, K. Ngamchuea, R.G. Compton, Simulated low-support voltammetry: deviations from Ohm's Law, J. Electroanal. Chem. 830–831 (2018) 88–94, https://doi.org/10.1016/J.JELECHEM.2018.10.032.
[41] M.G. Trachioti, A.C. Lazanas, M.I. Prodromidis, Shedding light on the calculation of electrode electroactive area and heterogeneous electron transfer rate constants at graphite screen-printed electrodes, Microchimica. Acta 190 (2023), https://doi.org/10.1007/s00604-023-05832-w.

Supplementary file

Oxygen Plasma-Tailored SPCEs for Enhanced Surface Reactivity and Electron Transfer: Toward Improved Electrodes

Sunil Luhar[1*,] *Kamila Sadowska* [1*,]

[1]*Nalecz Institute of Biocybernetics and Biomedical Engineering, Polish Academy of Sciences, Ks. Trojdena 4, 02--109 Warsaw, Poland*

***Corresponding author**: E-mail address: sluhar@ibib.waw.pl, ksadowska@ibib.waw.pl*

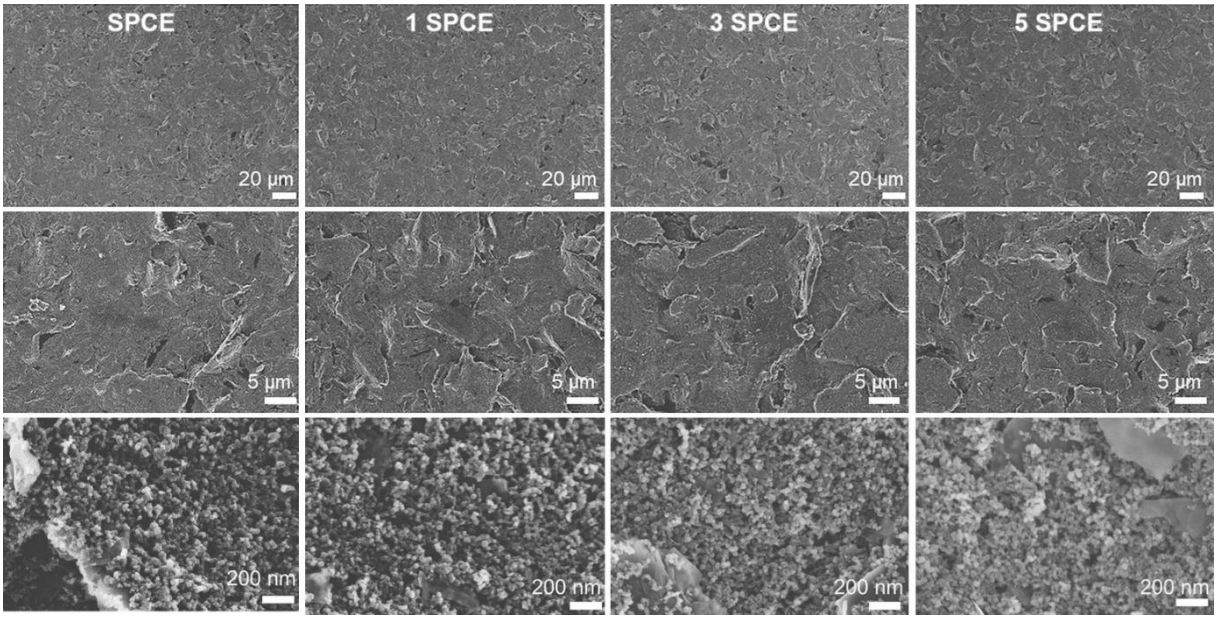

Figure S1. SEM images of pristine SPCE and plasma-treated samples (1 SPCE, 3 SPCE, and 5 SPCE) captured at different magnifications.

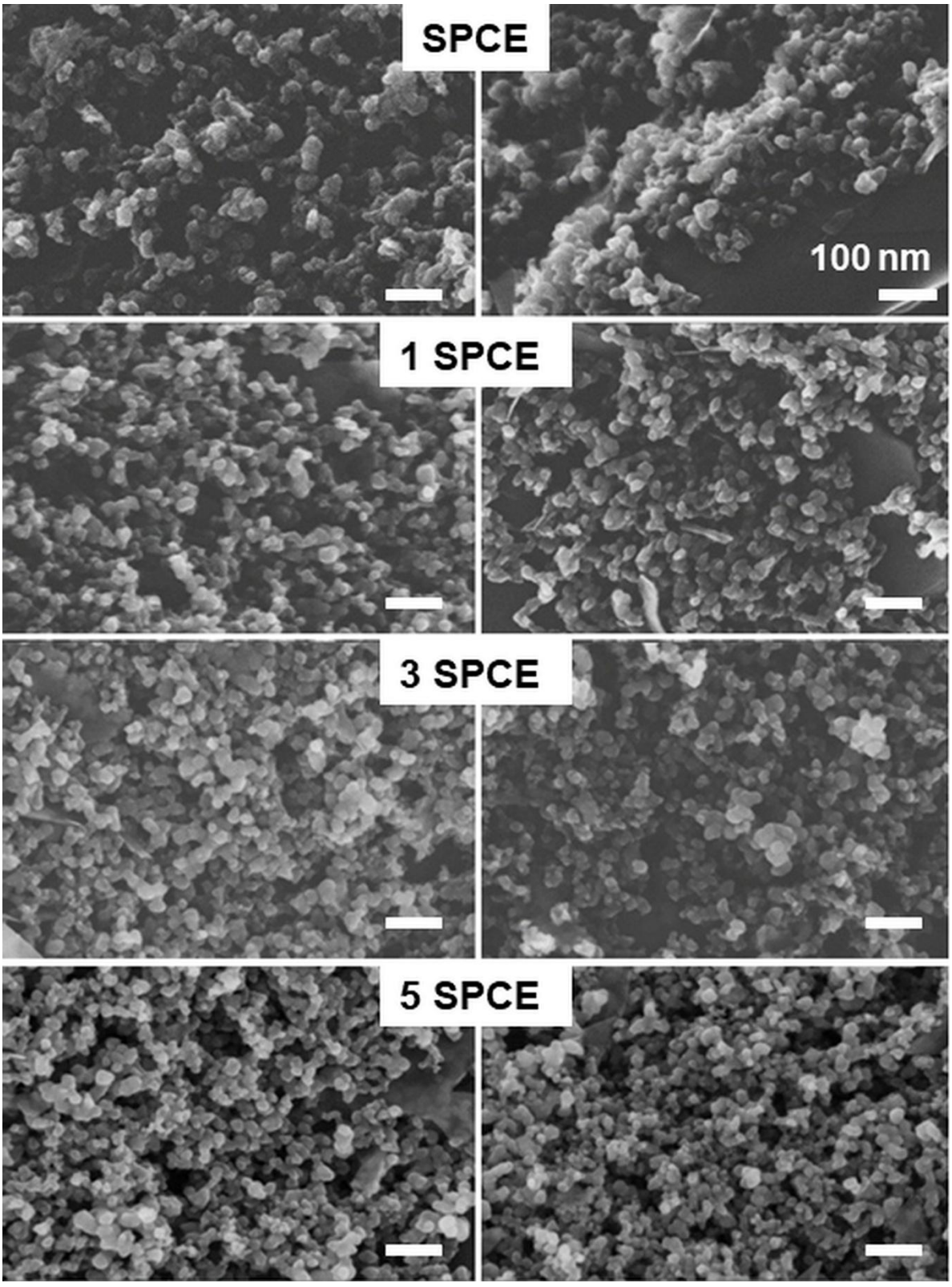

Figure S2. SEM images of pristine SPCE and plasma-treated samples (1 SPCE, 3 SPCE, and 5 SPCE) captured at the same magnification at different locations.

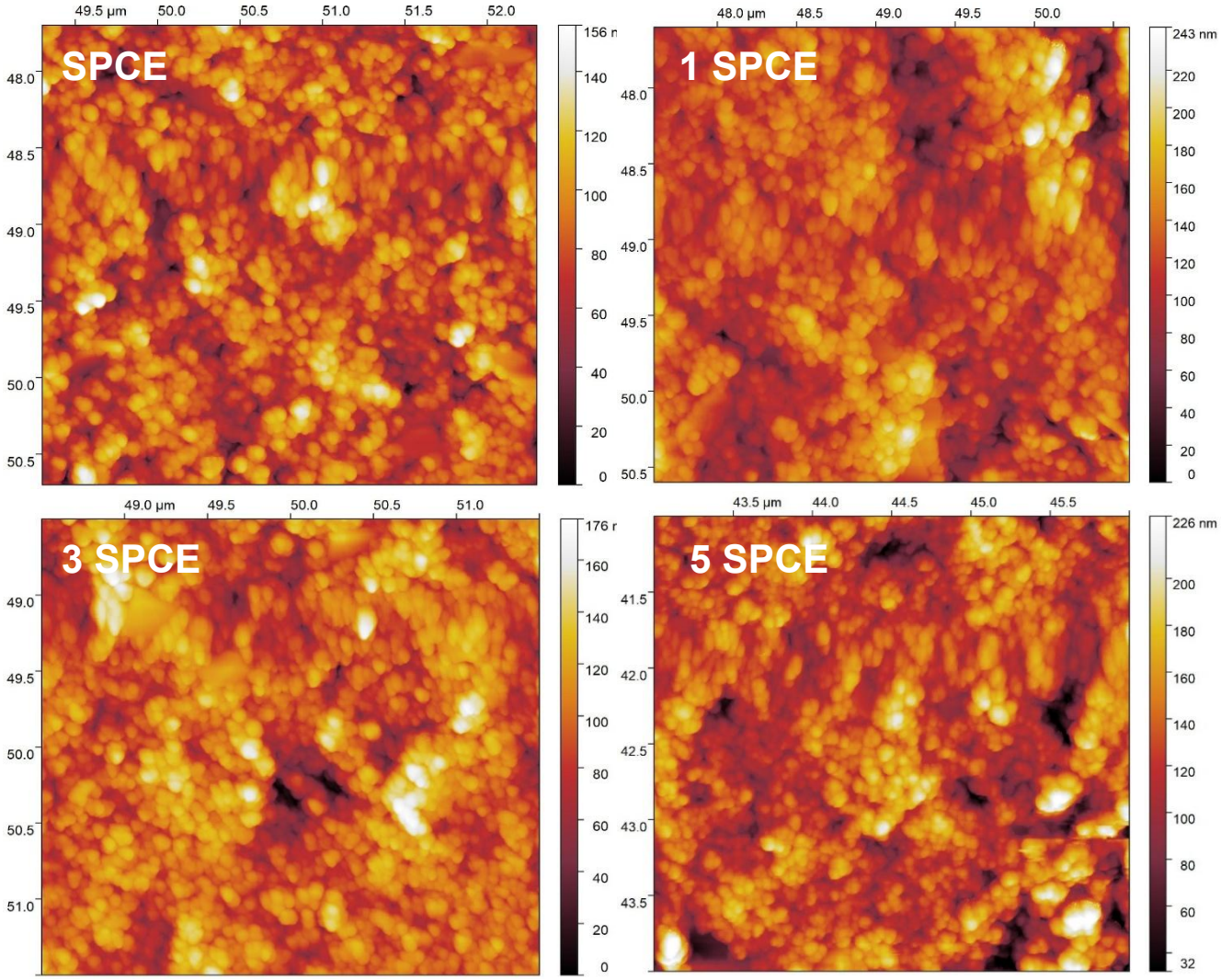

Figure S3. AFM images of pristine SPCE and plasma-treated samples (1 SPCE, 3 SPCE, and 5 SPCE).

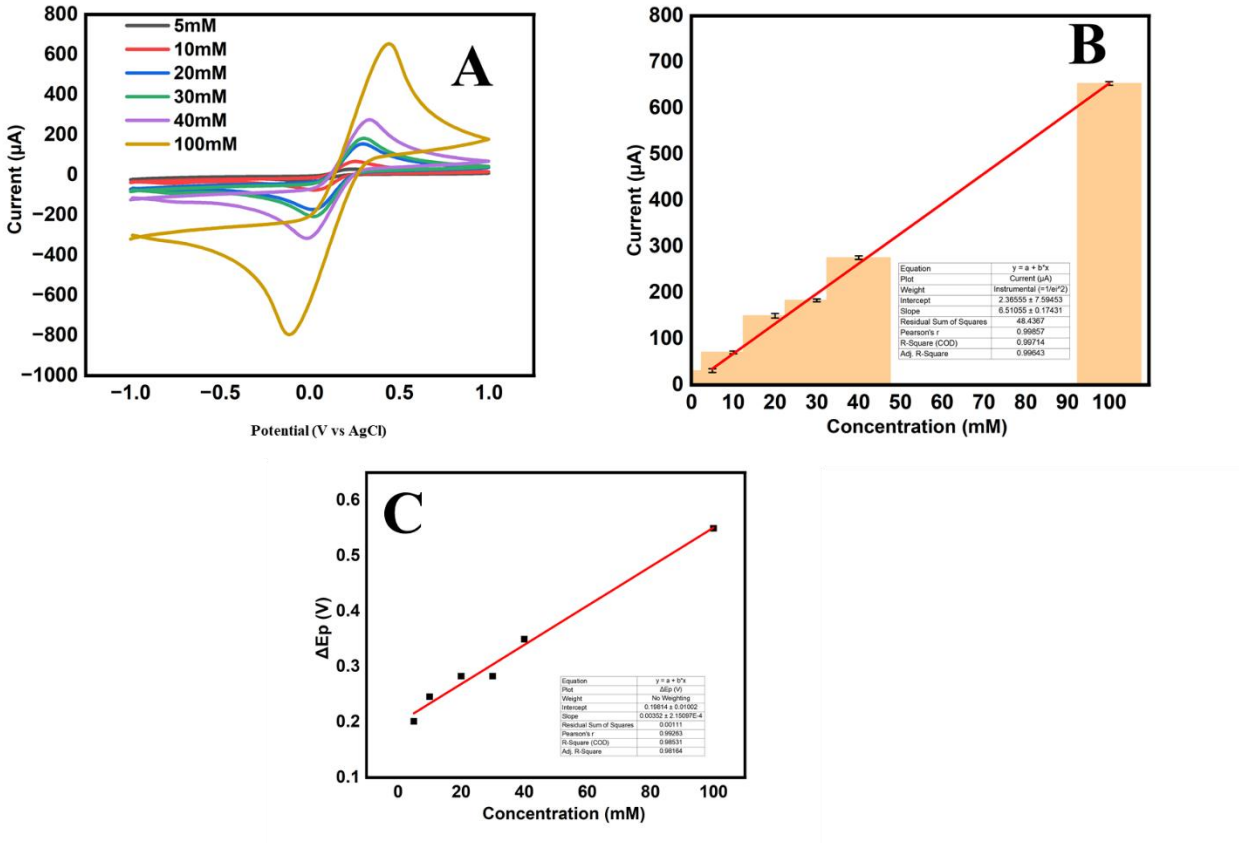

Figure S4. A) Cyclic voltammetry (CV) responses of screen-printed carbon electrodes (SPCEs) recorded in equimolar $K_3[Fe(CN)_6]/K_4[Fe(CN)_6]$ solutions with varying concentrations (5 mM to 100 mM) in 0.1 M KCl. Measurements were performed over a potential range of –1.0 V to +1.0 V at a scan rate of 50 mV/s. B) Calibration plot showing anodic peak currents as a function of $K_3[Fe(CN)_6]/K_4[Fe(CN)_6]$ concentration. C) Calibration plot potential differation of $K_3[Fe(CN)_6]/K_4[Fe(CN)_6]$ concentration Data are presented as mean ± standard deviation (n = 3), with error bars below 5%. Inset: linear regression curve with corresponding equation and R^2 value, demonstrating strong correlation and electrode sensitivity across the tested concentration range.

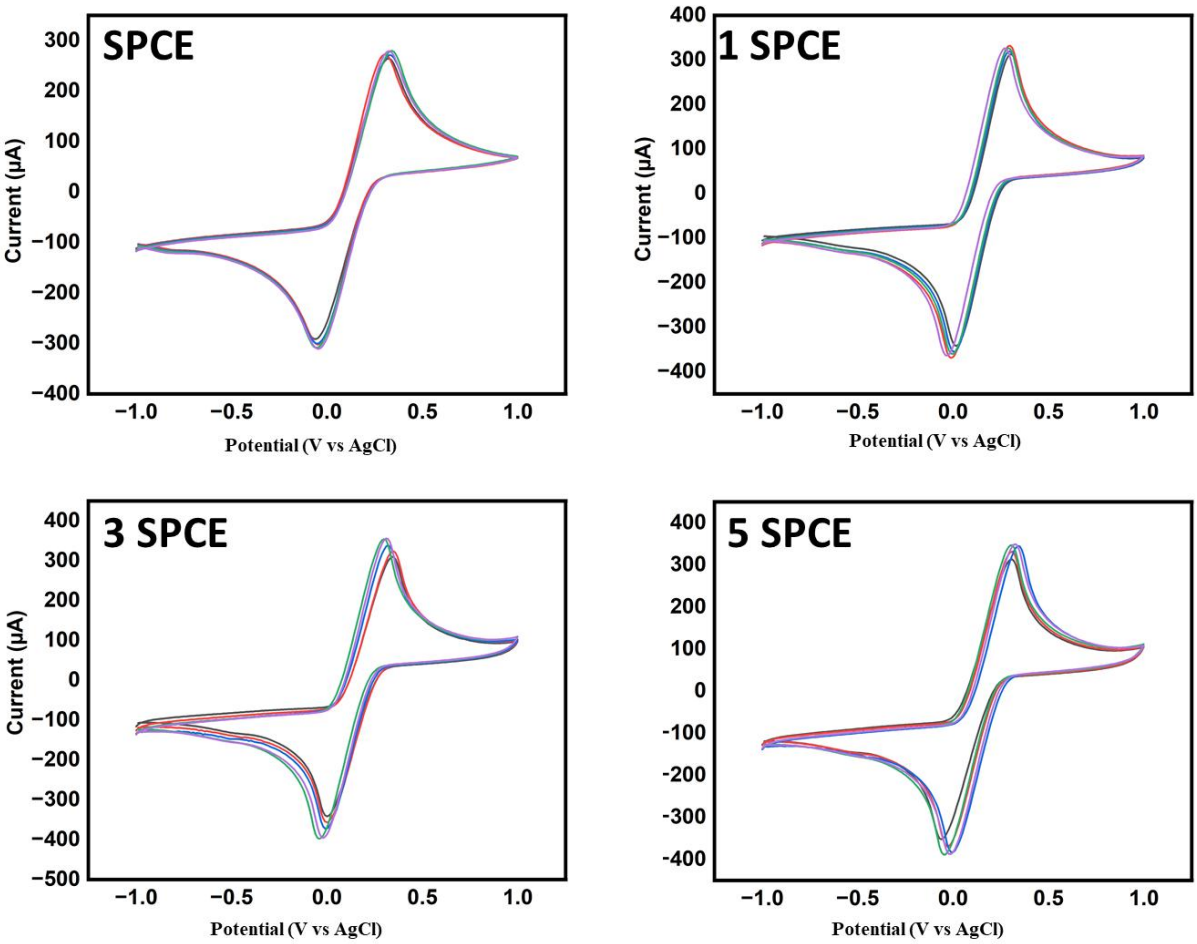

Figure S5. Cyclic voltammograms of SPCE, 1 SPCE, 3 SPCE, and 5 SPCE. Measurements were performed in an equimolar 40 mM solution of potassium ferricyanide/potassium ferrocyanide ($K_3[Fe(CN)_6]/K_4[Fe(CN)_6]$) solution containing 0.1 M KCl using a potential range of −1 V to +1 V at a scan rate of 50 mV/s. Each electrode was tested over five consecutive cycles to assess electrochemical behaviour and reproducibility.

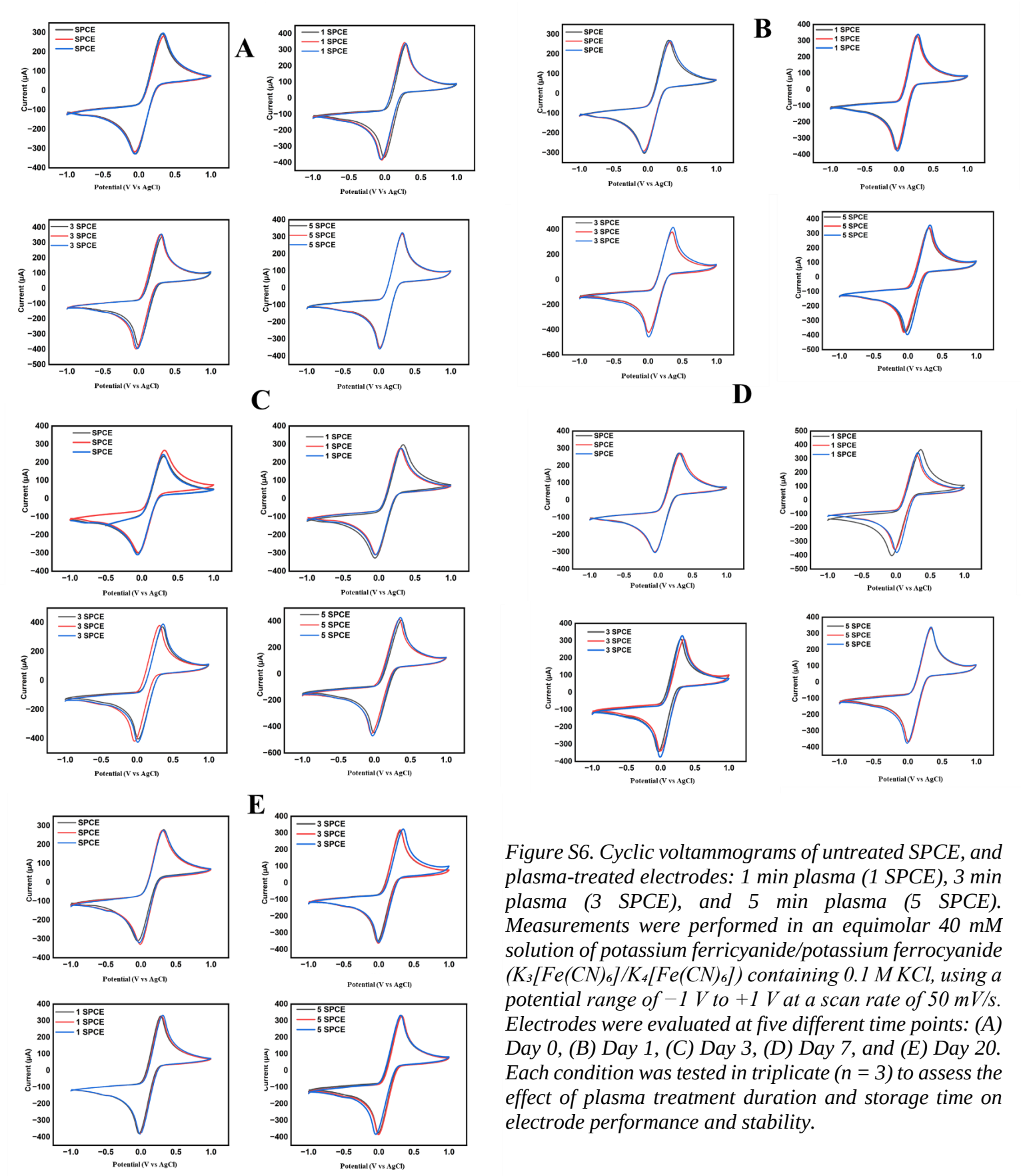

Figure S6. Cyclic voltammograms of untreated SPCE, and plasma-treated electrodes: 1 min plasma (1 SPCE), 3 min plasma (3 SPCE), and 5 min plasma (5 SPCE). Measurements were performed in an equimolar 40 mM solution of potassium ferricyanide/potassium ferrocyanide ($K_3[Fe(CN)_6]/K_4[Fe(CN)_6]$) containing 0.1 M KCl, using a potential range of −1 V to +1 V at a scan rate of 50 mV/s. Electrodes were evaluated at five different time points: (A) Day 0, (B) Day 1, (C) Day 3, (D) Day 7, and (E) Day 20. Each condition was tested in triplicate (n = 3) to assess the effect of plasma treatment duration and storage time on electrode performance and stability.